Particle Accelerators
1985 Vol. 16 pp. 155–170
0031-2460/85/1603-0155/$20.00/0

© Gordon and Breach, Science Publishers, Inc. and OPA Ltd.
Printed in the United States of America

THE EFFECT OF SPATIAL FIELD INDEX FLUCTUATIONS ON THE DYNAMICS OF A HIGH-CURRENT ELECTRON RING IN A MODIFIED BETATRON

C. AGRITELLIS,† S. J. MARSH‡ and C. A. KAPETANAKOS

SFP Advanced Accelerator
Plasma Physics Division
Naval Research Laboratory
Washington, D.C. 20375

(*Received January 3, 1984; in revised form March 20, 1984*)

Analytical and computer simulation results are reported on the effect of spatial fluctuations of the external-field index on the dynamics of a high-current electron ring in a modified betatron. These nonlinear studies clearly demonstrate that the external field-index fluctuations are, in general, harmless to the high-current ring. In addition, it was found that a small ($\sim 1\%$) temperature spread parallel to the direction of propagation excites oscillations in the rms emittance, but the amplitude of these oscillations is substantially lower than in a conventional betatron.

I. INTRODUCTION

The modified betatron belongs to the class of cyclic induction accelerators, i.e., the electrons are accelerating by an inductive electric field. So far three different cyclic induction accelerators have been proposed: the conventional betatron,[1–3] the modified betatron[4–14] and the stellatron.[15] The modified betatron includes, in addition to the time-varying betatron magnetic field that is responsible for the acceleration, a strong toroidal magnetic field that substantially improves the stability of the conventional betatron. In the stellatron, the addition of a stellarator field to the modified betatron substantially reduces the displacement of the orbit that is due to energy mismatch. However, beam trapping and resonances appear to be presently unsolved problems.

The linear dynamics of a high-current electron ring in a modified betatron geometry has been studied extensively[4–14] during the last few years. These studies are mainly motivated by extensive evidence suggesting that the modified betatron has the potential to confine high-current electron rings, even in the presence of a substantial transverse emittance.[16]

However, in any practical device, nonlinearities will be present and their effect on the dynamics of the beam should be carefully considered. The sources of nonlinearities in a high-current modified betatron are numerous. Probably the most important of these are: (i) large ring displacements from the minor axis of the torus, (ii) azimuthal perturbations in the magnetic fields, (iii) the gradient of the toroidal magnetic field,

† Science Applications, Inc., McLean, VA 22102
‡ Sachs-Freeman Associates, Bowie, MD 20715

(iv) non-uniform particles and current densities in the ring and (v) rapid field-index spatial variations.

The nonlinear dynamics of very tenuous electron rings in a modified betatron accelerator has been studied recently by Chernin.[17] His studies were limited to quadratic nonlinearities in the absence of self-fields and image fields from the surrounding walls. For azimuthally symmetric fields, he concluded that the quadratic nonlinearities are quite harmless to the electron ring.

In this paper, we use a computer simulation code to study the effect of several nonlinearities on the dynamics of the electron ring. The nonlinearities that are due to the azimuthal perturbations of the fields are not included in our studies. A substantial fraction of our effort is focused on the effect of the large spatial fluctuations of the field index. By comparing the electron-ring evolution in fields of constant field index n with that in fields of large $\partial n/\partial r$, it becomes clear that the field-index fluctuations are, in general, harmless to high-current rings. It should be noticed that $\partial n/\partial r$ in the simulation is larger than that expected to be present in the NRL modified betatron.

Additional conclusions to be drawn for our results are that a small ($\sim 1\%$) azimuthal temperature spread excites oscillations in the rms emittance, but the amplitude of these oscillations is substantially lower than in a conventional betatron.[16] Furthermore, a large emittance growth and beam expansion are observed when the electrons cross the single-particle resonance, i.e., when their frequency $\omega = 0$. The expansion of the beam can be effectively reduced by a large toroidal magnetic field.

II. COMPUTER SIMULATION RESULTS

a. Description of the Particle in Cell Computer Code

The computer code has been described previously.[11] Here we provide a very brief summary with emphasis on a recent modification related to the initial loading of the particles. Briefly, the particle simulation code is 2D in configuration and 3D in velocity space. It computes self-consistently all self fields, except the self B_θ field. This assumption is valid provided v/γ is small. In addition, the radiative term (displacement current) is ignored, i.e., the code uses the Darwin model for Maxwell's equations.

The electrostatic potential is computed from Poisson's equation

$$\nabla^2 \Phi = \rho/\epsilon_0, \tag{1}$$

and the magnetic vector potential from

$$\nabla^2 A_\theta - \frac{A_\theta}{r^2} = -\mu_0 J_\theta, \tag{2}$$

with the boundary condition $\Phi = A_\theta = 0$ at the conducting wall.

Equations (1) and (2) are solved by Fourier decomposition in the $z - r$ direction and then by Gaussian elimination of the resultant tridiagonal matrix of equations obtained from a 3-point differencing scheme for ∇_r^2. The inverse Fourier transform yields A_θ and Φ on the grid. The particle velocities in the toroidal direction are obtained using the conservation of cannonical momentum. Therefore, the equation for A_θ is not properly time centered because the velocities from the previous time step are used to calculate

the currents from the canonical momenta. This method was chosen primarily for its speed and simplicity, but care must be taken in applying the code when the inductive acceleration of particles in the toroidal direction is significant.

In several runs, the particles were loaded in the code at $t = 0$ using a cylindrical K-V distribution. In these runs, the electrons quickly acquired an "energy spread". This "thermalization" is due to the fact a cylindrical K-V distribution is not appropriate for high-current electron rings that have large aspect ratio r_0/r_b, where r_0 is the major and r_b the minor radius of the ring. The reason is that a cylindrical K-V distribution requires that the potential be the same on both the left and right side of the beam. However, in a actual ring there is a potential difference between the inner and outer edge. Thus, a ring that has been incorrectly initialized tries to attain a more physical distribution, but in the absence of dissipation this can be achieved only temporarily. In the process, a spread in γ is developed, which is equivalent to temperature. In all the results presented in this paper, the code was loaded at $t = 0$ correctly, i.e., taking into account the asymmetry of the potential across the ring.

b. Results Without Temperature in the Azimuthal Direction

Figure 1 shows the modified-betatron geometry and the system of coordinates that will be used in our subsequent discussion. The center of the electron ring is located away from the center of the minor cross-section of the torus and at a distance $\Delta = (\Delta r^2 + \Delta z^2)^{1/2}$. Results from the computer simulation are shown in Fig. 2. The various parameters for this run are listed in Table I. At $t = 0$, the 5-kA electron ring is located on the horizontal symmetry plane and at a distance $\Delta = 8$ cm, i.e., half-way between the minor axis and the wall of the toroidal chamber. It is apparent from the small variations of the ring envelope [Figs. 2a and 2b] that the ring is reasonably well matched. As shown in Table I, the external field index n is constant and equal to 0.42.

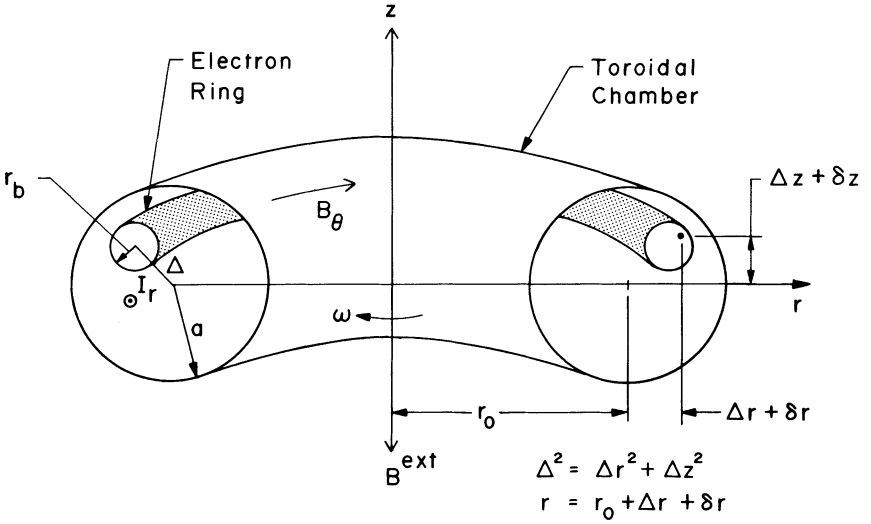

FIGURE 1 Modified-betatron configuration and system of coordinates.

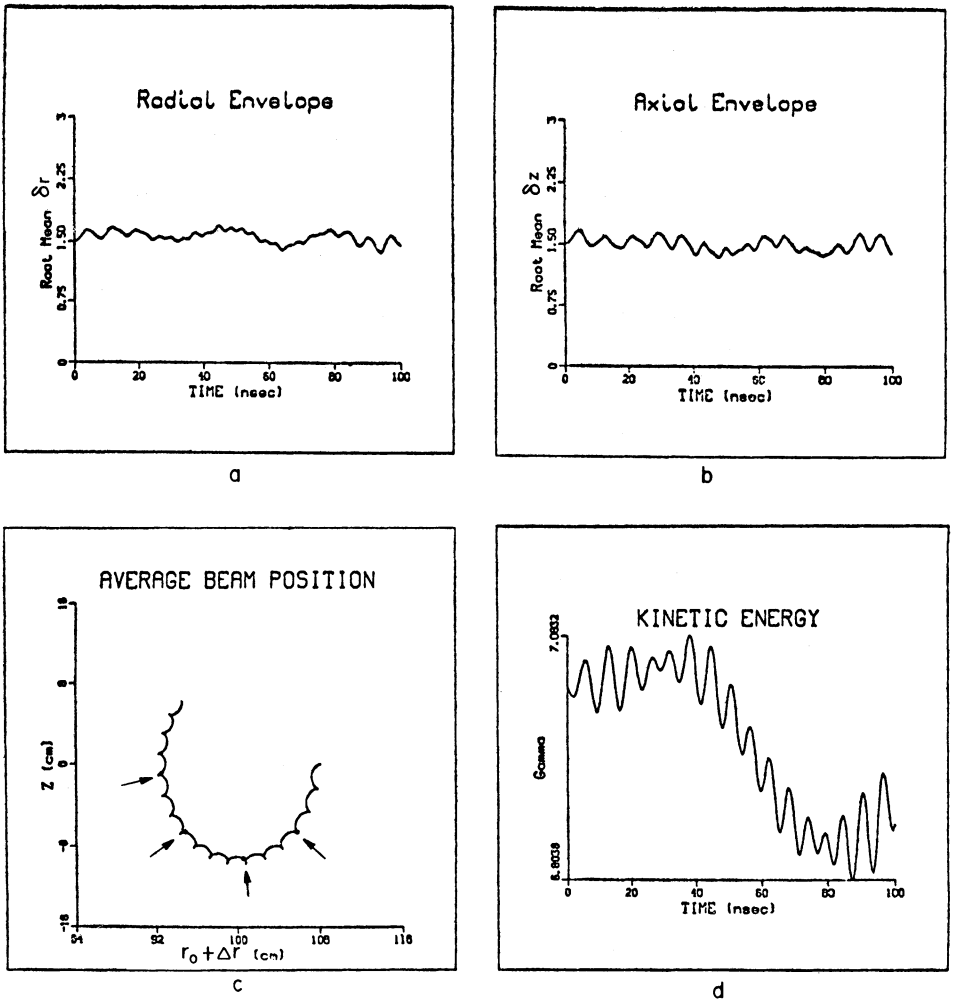

FIGURE 2 Temporal variation of the rms radial distance of electrons from the center of the minor cross section of the ring; (b) temporal variation of the rms vertical distance of electrons from the center of the minor cross section of the ring; (c) orbit of the ring's center in the r-z plane; (d) temporal variation of ring kinetic energy. In this run, the external-field index is uniform. The various parameters are listed in Table I.

For such a value of n, linear theory[11,13] predicts that the minor axis of the ring has two modes of oscillation, slow (bounce frequency) and fast (cyclotron frequency corresponding to the toroidal field). The orbit of the ring axis associated with the slow or bounce mode is approximately a circle that is centered around the ring equilibrium position. Although the run was terminated before the ring could complete a full bounce period, it is clear from Fig. 2c that the center of the ring describes an orbit that is similar to that predicted by the theory. Both modes of oscillation are quite apparent. The radius of the fast mode ρ_f can be computed approximately from the expression $\rho_f = v_\theta \epsilon_N / r_b \Omega_\theta$, where v_θ is the azimuthal velocity, ϵ_N is the normalized emittance, r_b is the ring radius and Ω_θ the cyclotron frequency of the local toroidal magnetic field. The time interval between two successive arrows in the figure is 20 nsec.

TABLE I

Parameters of the Run Shown in Fig. 2

Run No. M14D
Initial beam energy $\gamma_0 = 7.117$
Beam current I (KA) = 5 KA
Major radius r_0 (cm) = 100
Initial beam minor radius r_b (cm) = 3
Torus minor radius a (cm) = 16
Initial beam center position r_i (cm) = 108
Betatron magn. field at r_0, $z = 0$, B_{0z} (G) = 136.2
Toroidal magn. field at r_0, $z = 0$, $B_{0\theta}$ (G) = 388
Initial emittance ε (rad − cm) = 0.1
Initial temperature spread (half-width) $\frac{\Delta\gamma}{\gamma} = 0$
External field index $n = 0.42$ (Constant)
Self field index $n_s = 1.34$
Wall resistivity $\rho = 0$
Timd step (nsec) = 100 ps
No. of particles = 1024

The ring kinetic energy also oscillates with the two characteristic modes as may be seen in Fig. 2d. The variation of γ can be computed approximately by integrating the energy rate equation

$$mc^2 \frac{d\gamma}{dt} = -|e|\mathbf{v} \cdot \mathbf{E} = |e|v_\theta \frac{\partial A_\theta}{\partial t}, \tag{3}$$

using for the self magnetic vector potential the expression

$$A_\theta^s = \frac{2I_r}{c}\left(1/2 + \ln(a/r_b) + \ln(1 - \Delta^2/a^2)\right). \tag{4}$$

In Eq. (4), I_r is the ring current, a is the minor radius of the torus and Δ is the distance between the ring minor axis and that of the torus. It should be noticed that Eq. (4) does not include toroidal effects and therefore is valid only for low ν/γ rings.

Since $I_r = -|e|Nv_\theta/2\pi r$, where N is the total number of electrons in the ring and the external part of the magnetic vector potential remains constant, we get from Eqs. (3) and (4)

$$\gamma(t) - \gamma(0) = 2\nu_0 \left\{ \frac{r_0}{r(0)} [1/2 + \ln(a/r_b(0)) + \ln(1 - \Delta^2(0)/a^2)] - \frac{r_0}{r(t)} [1/2 + \ln(a/r_b(t)) + \ln(1 - \Delta^2(t)/a^2)] \right\}, \tag{5}$$

where ν_0 is the Budker parameter when the ring center is located at r_0, i.e.,

$$\nu_0 = \frac{N}{2\pi r_0} \frac{|e|^2}{mc^2}. \tag{6}$$

In the fast mode, γ changes through the transverse oscillations of the ring envelope.

Since in this fast time scale r and Δ remain approximately constant, Eq. (5) becomes

$$\gamma(t) - \gamma(0) = 2v_0 \frac{r_0}{r} \ln[r_b(t)/r_b(0)].$$

In the slow mode, γ changes mainly through the variation of the ring current, which results from the changing r. Since the contribution from the variation of r_b and Δ are in general small, Eq. (5) gives

$$\gamma(t) - \gamma(0) = 2v_0 r_0[1/2 + \ln(a/r_b(0)) + \ln(1 - \Delta^2(0)/a^2)][r(t) - r(0)]/r(t)r(0). \quad (7)$$

Equation (7) predicts that $\gamma(t)$ decreases with $r(t)$. In addition, for the results of Fig. 2d, Eq. (7) predicts a reduction in γ between $t = 0$ and $t = 80$ nsec of 0.18, which is in excellent agreement with the computer simulation results.

As was stated before, the run shown in Fig. 2 was made using a constant external-field index. The purpose of this run was to serve as a "bench mark" for the rest of the runs that were made with a variable external-field index. The radial profile of the betatron field and the variation of the external field index are shown in Fig. 3. The

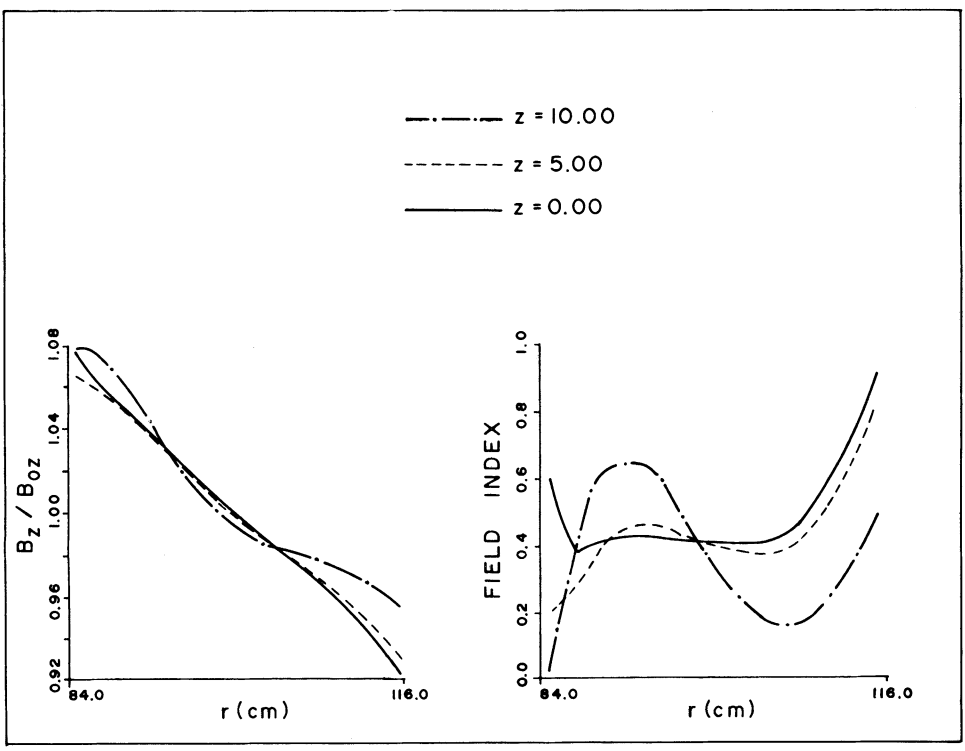

FIGURE 3 Variation of the betatron magnetic field and external-field index with radial distance at three vertical (z) positions.

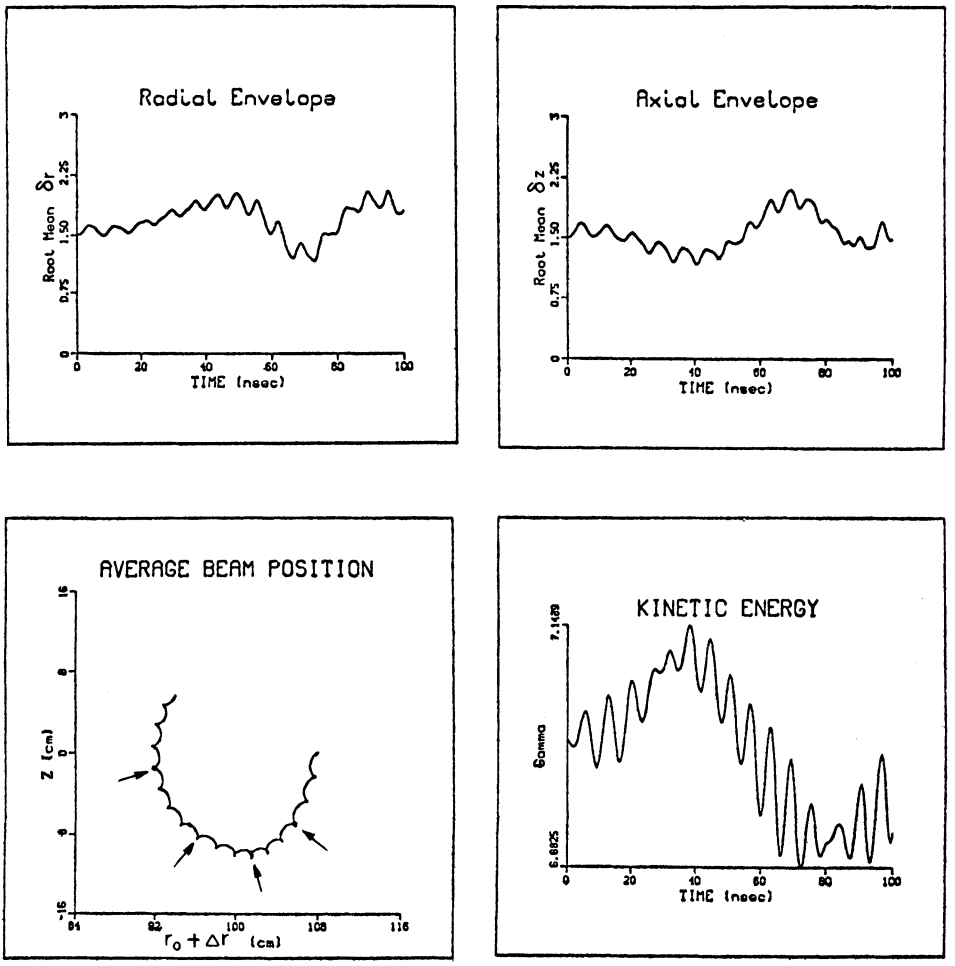

FIGURE 4 (a) Temporal variation of the rms radial distance of electrons from the center of the minor cross section of the ring; (b) temporal variation of the rms vertical distance of electrons from the center of the minor cross section of the ring; (c) orbit of the ring center in the r-z plane; (d) temporal variation of ring kinetic energy. In this run, the external-field index varies as shown in Fig. 3. The various parameters are listed in Table II.

assumed variation is in effect greater than that expected to be present in a well-designed device.

The effect of the external field-index variations on the dynamics of the ring is shown in Fig. 4. The parameters of this run are listed in Table II and, with the exception of the external-field index, are identical to those of run listed in Table I. By comparing Figs. (2) and (4), it may be concluded that the variation of the field index does not have a profound effect on the dynamics of the ring. Although some details are different, the gross features of the two runs are very similar. The most pronounced new feature of the results in Fig. 4 is the slow time-scale variation of the ring envelope. As the ring moves from its initial position at $z = 0$ to $z \neq 0$, the field index is reduced and the ring becomes unmatched, resulting in envelope oscillations.

TABLE II

Parameters of the Run Shown in Fig. 4

Run No. M16A
Initial beam energy $\gamma_0 = 7.117$
Beam current I (KA) = 5
Major radius r_0 (cm) = 100
Initial beam minor radius r_b (cm) = 3
Torus minor radius a (cm) = 16
Initial beam center position r_i (cm) = 108
Betatron magn. field at $r_0, z = 0$, B_{0z} (G) = 136.2
Toroidal magnetic field at $r_0, z = 0$, $B_{0\theta}$ (G) = 388
Initial emittance ϵ (rad − cm) = 0.1
Initial temperature spread (half-width) $\frac{\Delta\gamma}{\gamma} = 0$
External field index n = see Fig. 3
Self field index $n_s = 1.34$
Wall resistivity $\rho = 0$
Time step (nsec) = 100
No. of particles = 1024

Snapshots of the minor cross section of the ring and the magnetic field lines corresponding to the total magnetic field are shown in Fig. 5. As can be easily computed, the zero magnetic field point occurs at $\simeq r_b/2$.

Similar results to those shown in Fig. 4 were also obtained for smaller initial ring displacements $\Delta(0)$. Figure 6 shows the results for $\Delta(0) = 5$ cm. The parameters of this run are listed in Table III. In all the runs, we carefully avoided crossing the beam resonance, i.e., the radial frequency

$$\tilde{\omega}_r^2 = \left(\frac{\Omega_{0z}}{\gamma_0}\right)^2 [\xi^2 - n(t)\xi - n_s r_b^2/a^2],$$

where

$$\xi = [1 + 2(\nu/\gamma)(0.5 + \ln a/r_b)]^{-1},$$

was kept different than zero. The implications of crossing the resonance are presently under investigation.

c. *The Effect of Temperature*

In the system of coordinates shown in Fig. 1, the equations describing the motion of individual electrons in a constant-radius beam with $\Delta = 0$ having an azimuthal energy spread $\Delta\gamma/\gamma_0$ are

$$\delta\ddot{r} + \omega_r^2\,\delta r - (\Omega_{0\theta}/\gamma_0)\,\Delta\dot{z} = \frac{c^2}{r_0}\frac{\Delta\gamma}{\gamma_0}, \tag{8}$$

$$\delta\ddot{z} + \omega_z^2\,\delta z + (\Omega_{0\theta}/\gamma_0)\delta\dot{r} = 0, \tag{9}$$

where $\omega_r^2 = (\Omega_{0z}/\gamma_0)^2(1 - n - \tilde{n}_s)$, $\omega_z^2 = (\Omega_{0z}/\gamma_0)^2(n - n_s)$ and $\Delta\gamma = \gamma - \langle\gamma\rangle$ is

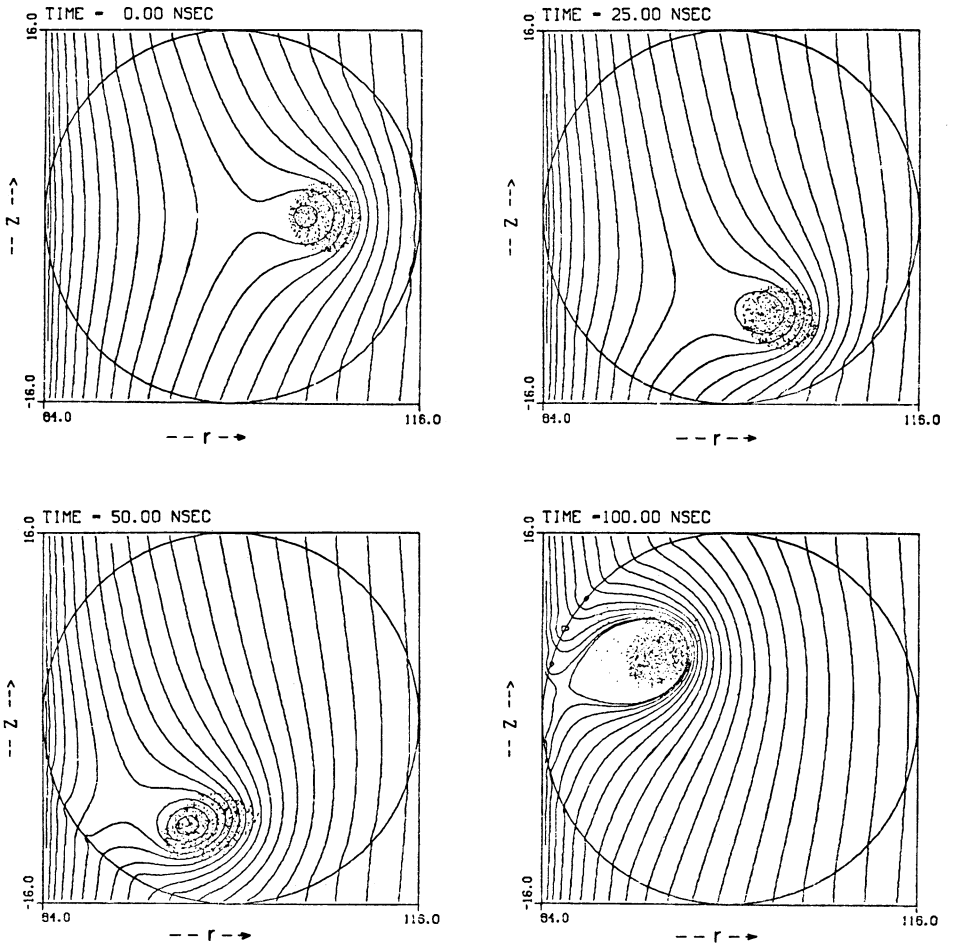

FIGURE 5 Snap-shots of the electron ring minor cross section and magnetic-field lines corresponding to the total magnetic field. The infinite-conductivity vacuum chamber has a circular minor cross section. The major axis of the torus is located to the left and at 100 cm from the center of the minor cross section of the torus. The various parameters are listed in Table II.

the azimuthal energy spread in the beam. Equations (8) and (9) do not include the toroidal corrections in the fields and therefore are valid only for low ν/γ_0 beams.

In the Larmor frame, i.e., a frame that rotates with a constant frequency $\Omega_L = 1/2(\Omega_{0\theta}/\gamma_0)$, Eqs. (8) and (9) take the form

$$\delta\hat{r}'' + K^2\,\delta\hat{r} = \frac{c^2}{r_0 v_\theta^2}\frac{\Delta\gamma}{\gamma_0}\cos\left(\frac{\Omega_L S}{v_\theta}\right), \tag{10}$$

$$\delta\hat{z}'' + K^2\,\delta\hat{z} = \frac{c^2}{r_0 v_\theta^2}\frac{\Delta\gamma}{\gamma_0}\sin\left(\frac{\Omega_L S}{v_\theta}\right), \tag{11}$$

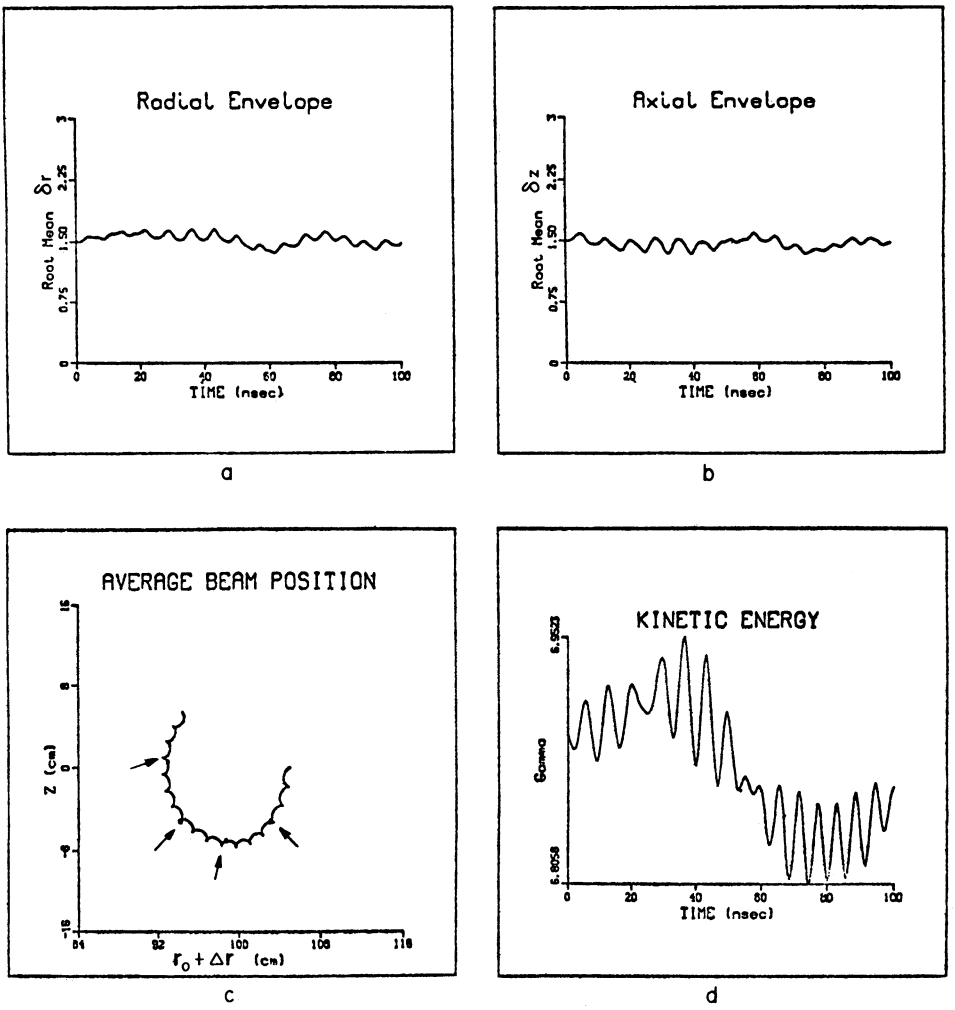

FIGURE 6 (a) Temporal variation of the rms radial distance of electrons from the center of the minor cross section of the ring; (b) temporal variation of the rms vertical distance of electrons from the center of the minor cross section of the ring; (c) orbit of the ring center in the r-z plane; (d) temporal variation of ring kinetic energy. In this run the external-field index varies as shown in Fig. 3. The parameters for this run are listed in Table III.

where

$$\delta\hat{r} = \cos\left(\frac{\Omega_L s}{v_\theta}\right)\delta r - \sin\left(\frac{\Omega_L s}{v_\theta}\right)\delta z,$$

$$\delta\hat{z} = \sin\left(\frac{\Omega_L s}{v_\theta}\right)\delta r + \cos\left(\frac{\Omega_L s}{v_\theta}\right)\delta z,$$

$K^2 = (\omega^2 + \Omega_L{}^2)/v_\theta{}^2$, $\omega^2 = \omega_r{}^2 = \omega_z{}^2$, i.e., $n = 1/2$, $\delta\hat{r}' = d\delta\hat{r}/ds$, $s = r_0\theta$ and θ is the toroidal angle.

TABLE III

Parameters of the Run Shown in Fig. 5

Run No. M05A
Initial beam energy $\gamma_0 = 6.994$
Beam current I (KA) = 4.76
Major radius r_0 (cm) = 100
Initial beam minor radius r_b (cm) = 3
Torus minor radius a (cm) = 16
Initial beam center position r_i (cm) = 105
Betatron magn. field at $r_0, z = 0$ B_{0z} (G) = 136.2
Toroidal magn. field at $r_0, z = 0$, $B_{0\theta}$ (G) = 388
Initial emittance ϵ (rad − cm) = 0.1
Initial temperature spread (half-width) $\frac{\Delta\gamma}{\gamma} = 0$
External field index n = see Fig. 3
Self field index $n_s = 1.33$
Wall resistivity $\rho = 0$
Time step (nsec) = 100 ps
No. of particles = 1024

Equations (10) and (11) describe forced oscillations and have a resonance at $\omega = 0$. The solution of Eqs. (10) and (11) when K is independent of s is

$$\delta\hat{r} = [\delta\hat{r}(0) - \delta r_0]\cos Ks + \frac{\delta\hat{r}'(0)}{K}\sin Ks + \delta r_0 \cos\left(\frac{\Omega_L s}{v_\theta}\right), \tag{12a}$$

and

$$\delta\hat{z} = \delta\hat{z}(0)\cos Ks + \frac{1}{K}[\delta\hat{z}'(0) - \delta r_0\Omega_L/v_\theta]\sin Ks + \delta r_0 \sin\left(\frac{\Omega_L s}{v_\theta}\right), \tag{12b}$$

where

$$\delta r_0 = \frac{c^2}{r_0\omega^2}\frac{\Delta\gamma}{\gamma_0}.$$

When $\omega = 0$, the solution of Eqs. (12) is

$$\delta\hat{r} = \delta\hat{r}(0)\cos\frac{\Omega_L s}{v_\theta} + \frac{v_\theta}{\Omega_L}\delta\hat{r}'(0)\sin\frac{\Omega_L s}{v_\theta} + \frac{c^2 s}{2r_0 v_\theta \Omega_L}\frac{\Delta\gamma}{\gamma}\sin\frac{\Omega_L s}{v_\theta}, \tag{13a}$$

and

$$\delta\hat{z} = \delta\hat{z}(0)\cos\frac{\Omega_L s}{v_\theta} + \frac{v_\theta}{\Omega_L}\delta\hat{z}'(0)\sin\frac{\Omega_L s}{v_\theta} + \frac{c2}{2r_0\Omega_L{}^2}\frac{\Delta\gamma}{\gamma}\left[\frac{\Omega_L s}{v_\theta}\cos\frac{\Omega_L s}{v_\theta} + \sin\frac{\Omega_L s}{v_\theta}\right]. \tag{13b}$$

In addition to the purely oscillatory terms, Eqs. (13) have two terms that make their amplitude increase with s. Therefore when $\omega = 0$ the beam radius will rapidly increase

and thus the model, which is based on r_b = constant, breaks down. Furthermore, n_s and ω are functions of r_b and thus neither remains constant as r_b increases. Therefore, in our subsequent discussion, we will assume that $\omega \neq 0$.

The rms beam emittance is defined by

$$\hat{\epsilon} = 4\{\langle \delta\hat{r}^2(t)\rangle\langle \delta\hat{r}'^2(t)\rangle - \langle \delta\hat{r}(t)\,\delta\hat{r}'(t)^2\}^{1/2}. \tag{14}$$

Substituting Eqs. (12a) and (12b) into Eq. (14) and taking averages over a K-V distribution, we obtain

$$\frac{\hat{\epsilon}^2}{16} = \langle \delta\hat{r}^2(0)\rangle\langle \delta\hat{r}'^2(0)\rangle + \delta r_0{}^2\{\langle \delta\hat{r}^2(0)\rangle[xK \sin Ks + x' \cos Ks]^2 + \langle \delta\hat{r}'^2(0)\rangle[x \cos Ks - \frac{x'}{K} \sin Ks]^2\}, \tag{15}$$

where

$$\left.\begin{aligned} x &= \cos\left(\frac{\Omega_L s}{v_\theta}\right) - \cos Ks \\ x' &= -\frac{\Omega_L}{v_\theta} \sin\left(\frac{\Omega_L s}{v_\theta}\right) + K \sin Ks \end{aligned}\right\} \text{for the } r\text{-component} \tag{16}$$

and

$$\left.\begin{aligned} x &= \sin\left(\frac{\Omega_L s}{v_\theta}\right) - \left(\frac{\Omega_L}{K v_\theta}\right) \sin Ks \\ x' &= \left(\frac{\Omega_L}{v_\theta}\right) \cos\frac{\Omega_L s}{v_\theta} - \left(\frac{\Omega_L}{v_\theta}\right) \cos Ks \end{aligned}\right\} \text{for the } z\text{-component} \tag{17}$$

If the initial conditions are such that

$$K^2\langle \delta\hat{r}^2(0)\rangle = \langle \delta\hat{r}'^2(0)\rangle,$$

Eq. (15) becomes

$$\frac{\hat{\epsilon}^2}{16} = \langle \delta\hat{r}^2(0)\rangle\langle \delta\hat{r}'^2(0)\rangle + \delta r_0{}^2 K^2\langle \delta\hat{r}^2(0)\rangle[x^2 + x'^2/K^2]. \tag{18}$$

When $\Omega_L{}^2 \gg \omega^2$, the two components of the rms emittance become

$$\frac{\hat{\epsilon}_r{}^2}{16} = \langle \delta\hat{r}^2(0)\rangle\langle \delta\hat{r}'^2(0)\rangle + 2(\delta r_0 \Omega_L / v_\theta)^2\langle \delta\hat{r}^2(0)\rangle\left[1 - \cos\left(\frac{\omega^2 s}{\Omega_{0\theta} v_\theta}\right)\right], \tag{19}$$

and

$$\frac{\hat{\epsilon}_z^{\,2}}{16} = \langle \delta\hat{z}^2(0)\rangle\langle \delta\hat{z}'^2(0)\rangle + 2(\delta r_0 \Omega_L / v_\theta)^2 \langle \delta\hat{z}^2(0)\rangle \left[1 - \cos\left(\frac{\omega^2 s}{\Omega_{0\theta} v_\theta}\right)\right]. \quad (20)$$

Since $\omega^2 s/\Omega_{0\theta} v_\theta \to 0$ when $\Omega_{0\theta} \gg \omega$, the amplitude of the oscillatory terms is very small. This is contrary to the conventional betatron, in which very small energy spread results in very large oscillations of the rms emittance.[16]

Results from the computer simulation with a small parallel temperature spread are shown in Fig. 7. The various parameters for this run are listed in Table IV. When a

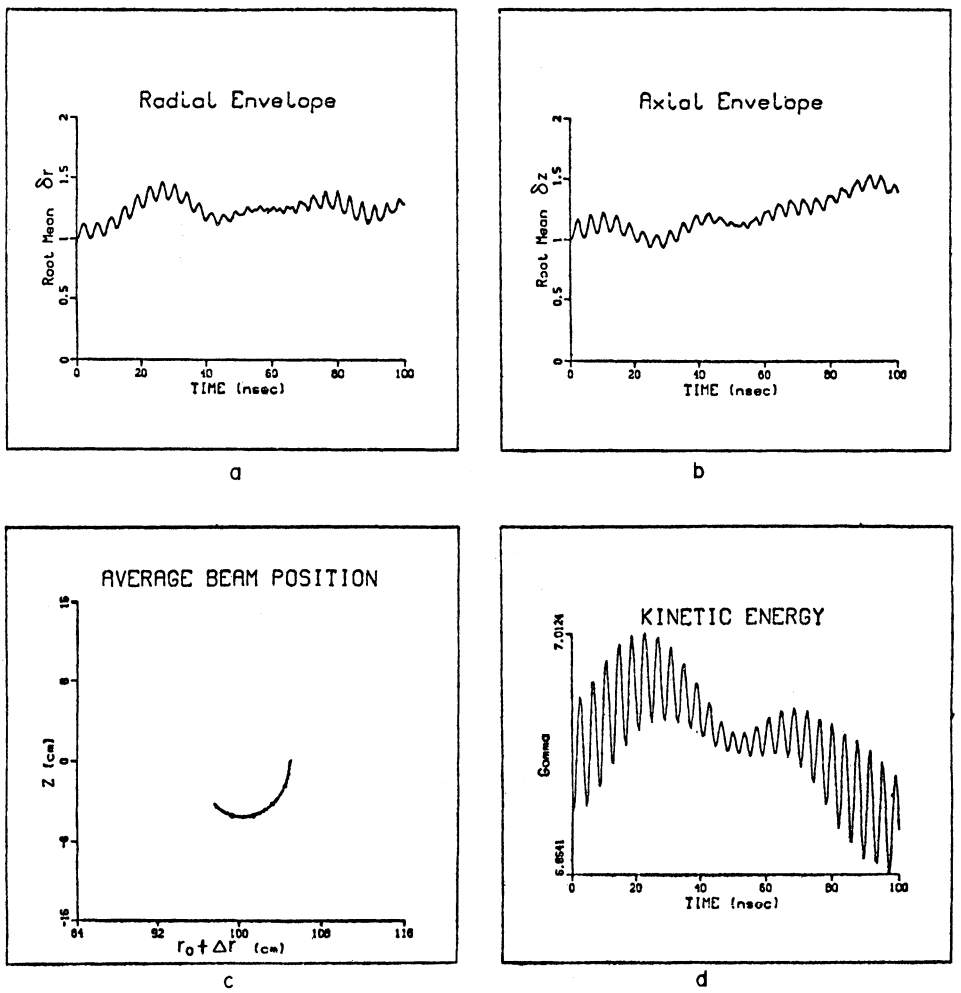

FIGURE 7 (a) Temporal variation of the rms radial distance of electrons from the center of the minor cross section of the ring; (b) temporal variation of the rms vertical distance of electrons from the center of the minor cross section of the ring; (c) orbit of the ring's center in the r-z plane; (d) temporal variation of ring kinetic energy. In this run the external-field index is uniform, but the electrons have a 1% (half-width) temperature spread along the toroidal direction. The various parameters for this run are listed in Table IV.

TABLE IV

Parameters of the Run Shown in Fig. 7

Run No. J02A
Initial beam energy $\gamma_0 = 7.004$
Beam current I (KA) = 5 KA
Major radius r_0 (cm) = 100
Initial beam minor radius r_b (cm) = 2
Torus minor radius a (cm) = 16
Initial beam center position r_i (cm) = 105
Betatron magn. field at r_0, $z = 0$, B_{0z} (G) = 140
Toroidal magn. field at r_0, $z = 0$, $B_{0\theta}$ (G) = 725
Initial emittance ϵ (rad − cm) = 0.1
Initial temperature spread (half-width) $\frac{\Delta\gamma}{\gamma} = 1\%$
External field index $n = 0.42$
Self field index $n_s = 2.984$
Wall resistivity $\rho = 0$
Time step (nsec) = 100 ps
No. of particles = 1024

parallel energy spread is present, the matching becomes more difficult and the beam envelope starts to oscillate. These oscillations result in the growth of the ring rms emittance and are discussed later.

The ring dynamics in the presence of temperature is similar to that in the absence of temperature, provided that even with the expansion of the beam radius, ω^2 remains different than zero. In one run, the various parameters were assigned values such that ω^2 would go through zero after a small expansion of the beam radius. A very rapid increase in the beam envelope was observed that was accompanied by a large growth of the rms emittance in approximately 100 nsec. However, the expansion had no noticeable effect on the macroscopic motion of the center of the beam, at least for the duration of the run.

The large expansion of the beam envelope that has been observed in this run is related to the unrealistically low value of the toroidal magnetic field used. Since reliable numerical analysis requires several cells across the minor cross-section of the ring, it was necessary to work with large minor radius rings, which can be matched only at low toroidal magnetic field. Specifically, the applied matching field for the 3-cm minor radius, 5-kA ring is 388G, at least five times smaller than that contemplated for the NRL modified betatron.

According to Eqs. (13), the terms with amplitude that increases linearly with s also vary in inverse proportion with B_θ. Therefore a large toroidal field can effectively reduce the expansion of the beam when the single-particle resonance ($\omega = 0$) is crossed.

The rms emittance as a function of time for $T_{11} \neq 0$ is shown in Fig. 8a. The various parameters are listed in Table IV. The corresponding result for $T_{11} = 0$ is shown in Fig. 8b. With the exception of the temperature, the various parameters for this run are identical to those listed in Table IV. Since in the numerical results

$$\langle \delta\hat{r}^2(0) \rangle = \langle \delta\hat{z}^2(0) \rangle,$$

and

$$\langle \delta\hat{r}'^2(0) \rangle = \langle \delta\hat{z}'^2(0) \rangle,$$

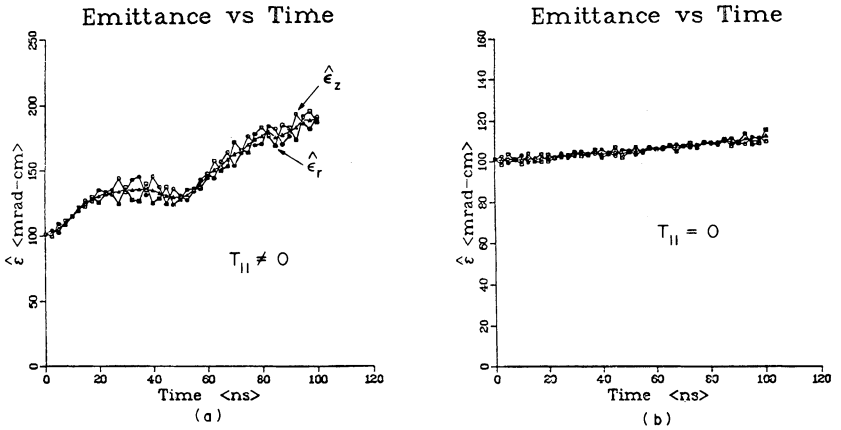

FIGURE 8 (a) Temporal variation of the rms emittance $\hat{\epsilon}_r$, ϵ_z and their average $(\hat{\epsilon}_r + \hat{\epsilon}_z)/2$, when there is a 1% (half-width) temperature spread T_{11} in the toroidal direction. The various parameters for this run are listed in Table IV; (b) as in (a) but with $T_{11} = 0$.

Eqs. (19) and (20) predict that

$$\epsilon_r \cong \pm \epsilon_z,$$

i.e., ϵ_r and ϵ_z are either in phase or approximately 180° out of phase. Figure 8a shows that ϵ_r and ϵ_z are 180° out of phase. This appears to be a general result and has been observed in all the runs with temperature or equivalent temperature.

The secular emittance growth in Fig. 8a is attributed to the radial expansion of the ring. This is also a general result and is observed in all unmatched rings with or without temperature. Among the various nonlinearities, such as field fluctuations, wall, density and radial expansion, the last appears to be the most pronounced.

III. CONCLUSIONS

Some preliminary experimental results[18] together with the extensive equilibrium[5–14] and stability analysis[19–24] indicate that the modified-betatron concept has the potential to lead to the development of a cyclic, high-current accelerator.

Confidence in the modified-betatron concept is further enhanced by the present results, which show that spatial fluctuations of the magnetic-field index that are inevitable in any practial device appear to be harmless to the high-current ring.

REFERENCES

1. D. W. Kerst, *Nature*, **157,** 90 (1940).
2. D. W. Kerst, *et. al., Rev. Sci. Inst.*, **21,** 462 (1950).
3. A. I. Paulovskii, *et al., Sov. Phys. Tech. Phys.*, **22,** 218 (1977).
4. A. G. Bonch-Osmolovskii, G. V. Dolbilow, I. N. Ivanov, E. A. Perelshtein, V. P. Sarantsev and O. I. Yarkovoy, JINR-Report P9-4135 Dubna (USSR) 1968.
5. P. Sprangle and C. A. Kapetanakos, *J. Appl. Phys.*, **49,** 1 (1978).
6. N. Rostoker, *Comments on Plasma Physics*, Gordon and Breach Science Publ. Inc. Vol. 6, p. 91 (1980).

7. C. L. Olson and V. Schumacher, *Collective Ion Acceleration*, Springer-Verlag, Berlin, Heidelberg, New York 1979, page 199.
8. P. Sprangle, C. A. Kapetanakos and S. J. Marsh, Proc. of the Intern. Top Conf. on High-Power Electron and Ion Beam Research and Technology; Palaiseau, France, June 29–July 3, 1981, p. 803; also NRL Memo Report 4666 (1981).
9. G. Barak, D. Chernin, A. Fisher, H. Ishizuda and N. Rostoker, Proc. of the Intern. Top. Conf. on High Power Electron and Ion Beam Research and Technology; Palaiseau, France, June 29–July 3, 1981, p. 795.
10. C. A. Kapetanakos, P. Sprangle and S. J. Marsh, NRL Memo Report 4835 (1982); also *Phys. Rev. Lett.*, **49**, 741 (1982).
11. C. A. Kapetanakos, P. Sprangle, D. P. Chernin, S. J. Marsh and I. Haber, NRL Memo Report 4905 (1982); also *Phys. Fluids*, **26,** 1634 (1983).
12. W. M. Manheimer and J. M. Finn, *Particle Accelerators* (1983).
13. D. P. Chernin and P. Sprangle, *Particle Accelerators*, **12,** 85 (1982).
14. G. Barak and N. Roskoker, *Phys. of Fluids*, **26,** 3 (1983).
15. C. Roberson, A. Mondelli and D. Chernin, *Phys. Rev. Lett.*, **50**, 507 (1983).
16. C. A. Kapetanakos, P. Sprangle and S. J. Marsh, NRL Memo Report 5108 (1983); also *Part. Accelerators* (1983).
17. D. Chernin, NRL Memo Report 5061 (1983), and *Particle Accelerators*, **14,** 139 (1984).
18. H. H. Fleischmann, D. Taggart, M. Parker and H. J. Hopman, Particle Accel. Conf. Bull. page 146 Santa Fe, NM, 21–23 March (1983), (this ref. describes a plasma betatron, in which the electron ring is neutralized).
19. P. Sprangle and J. Vomvoridis, NRL Memo Report 4688 (1981).
20. H. S. Uhm and R. C. Davidson, MIT, Plasma Fusion Center Report No. JA-81-30 (1981).
21. R. C. Davidson and H. S. Uhm, *Phys. Fluids*, **25,** 2089 (1982).
22. T. P. Hughes and B. B. Godfrey, Mission Research Corp. Report No. AMRC-R 354, 1982; also AMRC-R-332, 1982.
23. P. Sprangle and D. Chernin, NRL Memo Report 5176 (1983).
24. P. Sprangle and C. A. Kapetanakos, NRL Memo Report 4950 (1983); also *Particle Accelerators* (1983).